

Effect of Constraint on Creep Behavior of 9Cr-1Mo Steel

SUNIL GOYAL, K. LAHA, C.R. DAS, S. PANNEERSELVI, and M.D. MATHEW

The effect of constraint on creep rupture behavior of 9Cr-1Mo steel has been investigated. The constraint was introduced by incorporating a circumferential U-notch in a plain cylindrical creep specimen of 5 mm diameter. The degree of constraint was increased by decreasing the notch root radius from 5 to 0.25 mm. Creep tests were conducted on plain and notched specimens at stresses in the range of 110 to 210 MPa at 873 K (600 °C). The creep rupture life of the steel was found to increase under constrained conditions, which increased with the increase in degree of constraint and applied stress, and tended to saturate at a higher degree of constraint. The creep rupture ductility (pct reduction in area) of the steel was found to be lower under constrained conditions. The decrease in creep ductility was more pronounced at a higher degree of constraint and lower applied stresses. Scanning electron microscopic studies revealed a change in fracture behavior with stress and degree of constraint. The fracture surface appearance for relatively lower constrained specimens at higher stresses was predominantly transgranular dimple. Creep cavitation-induced intergranular brittle fracture near the notch root was observed for specimens having a higher degree of constraint at relatively lower stresses. The creep rupture life of the steel under constrained conditions has been predicted based on the estimation of damage evolution by continuum damage mechanics coupled with finite element analysis of the triaxial state of stress across the notch. It was found that the creep rupture life of the steel under constrained conditions was predominantly governed by the von-Mises stress and the principal stress became progressively important with increase in the degree of constraint and decrease in applied stress.

DOI: 10.1007/s11661-013-2025-z

© The Minerals, Metals & Materials Society and ASM International 2013

I. INTRODUCTION

COMPONENTS operating under creep conditions are often subjected to constrained creep deformation imposed by a sudden change in thickness/cross section, geometry, *etc.*, and also by a steep change in microstructure, having an appreciably different creep deformation resistance as in the fusion welded joints. In a laboratory experiment to study the effect of constraint on creep deformation, notches are usually introduced in creep specimens.^[1–6] Different creep rates across the notch root because of continuous changes in cross-sectional area impose a constraint on creep deformation to maintain the strain continuity. The degree of constraint imposed on the materials depends on the kind of notch introduced and the profile of the notch root and ductility of the material.^[7,8] Both V- and U-notches are incorporated in the cylindrical creep specimen to study the effect of constraint on creep behavior.^[8] Circumferential V-notches are found to exhibit a higher degree of constraint than that of circumferential U-notches.^[8] For laboratory experiments to study the effect of constraint on creep deformation and fracture, U-notches are

preferred over the V-notches, since the U-notches produce creep cavitation over a relatively larger volume, assisting the investigation.^[9]

The presence of notches may exhibit notch creep strengthening or weakening depending on the notch shape and acuity (ratio of diameter of minimum cross section to radius of notch root), testing conditions, and the material ductility.^[2–4,10] Notch strengthening is expected when the high axial stresses across the notch throat plane redistribute quickly below the applied stress. This kind of behavior is typically observed in ductile materials. However, notch weakening is expected in situations where the very high axial stresses due to the presence of the notch redistribute very slowly and the local accumulated strain exceeds the limit which is required for fracture before attaining the stationary state across the notch throat plane. This behavior is typically observed in brittle materials.

The stresses around the notch redistribute during creep deformation and approach a stationary state condition.^[8,11] Finite element (FE) analysis coupled with continuum damage mechanics (CDM) has been extensively used by many researchers to understand the stress redistribution and damage accumulation across the notch under creep conditions.^[12–15] It was observed that for each notch geometry, there is a skeletal point where the stresses are almost constant irrespective of the value of stress exponent n in Norton's law relating steady state creep rate ($\dot{\epsilon}_s$) with applied stress as $\dot{\epsilon}_s = A\sigma^n$, with A and n as material constants.^[11] The stresses at skeletal

SUNIL GOYAL and C.R. DAS, Scientific Officers, K. LAHA, Head, Creep Studies Section, S. PANNEERSELVI, Scientific Assistant, and M.D. MATHEW, Head, are with the Mechanical Metallurgy Division, Metallurgy and Materials Group, Indira Gandhi Centre for Atomic Research, Kalpakkam 603 102, India. Contact e-mail: goyal@igcar.gov.in

Manuscript submitted May 2, 2013.

Article published online October 12, 2013

Table I. Chemical Composition of the Material (wt pct)

Material	C	Si	Mn	P	S	Cr	Mo	Fe
9Cr-1Mo steel	0.1	0.49	0.46	0.008	0.002	8.36	0.93	bal

point obtained from FE analysis have been used to characterize the deformation and failure behavior of the material under triaxial creep conditions.^[15–21] The failure under triaxial state of stress is associated with the creep cavity nucleation and their growth, which depends on the distribution of stresses across the notch. A number of models^[1,19,22–24] have been proposed to account for the roles of different components of triaxial stress in governing the nucleation and growth of creep cavities and rupture life prediction. Among those, the most widely accepted ones are by Cane^[22] and Hayhurst^[1] relating the contribution of von-Mises stress and maximum principal stress in representative stress for prediction of rupture life under a triaxial state of stress under creep conditions.

Though there exists literature on experiments and modeling of creep behavior in the presence of relatively shallow notches,^[14,15,18] little exists on experiments and validation of such models for relatively sharper notches as well as on the effect of systematic variation in notch sharpness.^[3,17] In the present investigation, the effect of constraint on creep deformation of 9Cr-1Mo steel has been studied by incorporating circumferential U-notches having different notch acuity ratios in cylindrical creep specimens. The renewed interest in the creep behavior of 9Cr-1Mo steel is because of its possible uses as in-core applications as a wrapper material of sodium-cooled fast nuclear reactors.^[25,26] FE analysis has been carried out to estimate the stress distribution across the notch throat plane. The creep damage and rupture life estimation of notched specimens was carried out based on the FE analysis coupled with CDM and has been correlated with the fracture behavior of the material.

II. EXPERIMENTAL

A. Material and Creep Experiments

Creep tests were carried out on a plain cylindrical specimen of the 9Cr-1Mo steel at 873 K (600 °C) and at stresses in the range of 110 to 210 MPa in air. The blanks were given a heat treatment of normalizing [1223 K (950 °C) for 15 minutes followed by air cooling] and tempering [1053 K (780 °C) for 120 minutes followed by air cooling]. The plain creep specimens were of 5 mm diameter and 50 mm gage length. Chemical composition of the steel is given in Table I. The effect of constraint on creep behavior of the steel has been studied by carrying out creep tests at net stresses in the range of 110 to 210 MPa and 873 K (600 °C) on circumferentially U-notched specimens having a notch root radius of 1.25 mm with a notch throat diameter of 5 mm. Further, in order to study the effect of degree of constraint on creep behavior, creep tests were also carried out on circumferentially U-notched specimens

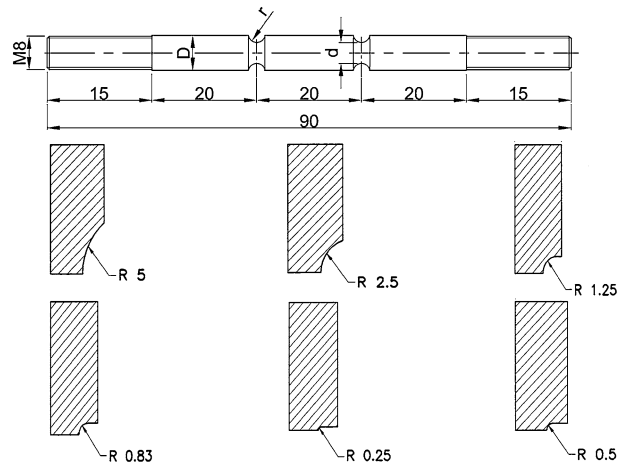


Fig. 1—Design of cylindrical notch creep specimens of different root radii for creep test.

Table II. Dimensions of Different Notch Geometries

D	8.35 mm
d	5.0 mm
r	5.0 to 0.25 mm

having various notch root radii in the range of 0.25 to 5 mm by keeping the notch throat diameter 5 mm at a net stress of 150 MPa and at 873 K (600°C). The geometry of the notched specimens is illustrated in Figure 1. The ratio of diameter of the parallel portion of the specimen to the notch throat diameter (D/d) was fixed at 1.67, see Table II. The variation of notch acuity ratio (d/r) from 1 to 20 resulted in an elastic stress concentration ranging from 1 to 3.4.

Creep specimens with two similar notches around 20 mm apart (Figure 1) were used for creep tests and the unfailed notch after creep test was utilized for a post-test metallographic investigation for creep damage evaluation. Fractography of both the plain and notched specimens was carried out employing a scanning electron microscope (SEM). Creep ruptured specimens were sectioned longitudinally, and mechanically polished and etched with Vilella's reagent (1 g picric acid and 5 mL hydrochloric acid in ethanol) for carrying out the SEM investigation for creep damage evaluation.

B. FE analysis of Stress Distribution

Finite element analysis of stress distribution across the notch throat plane during creep exposure has been carried out to understand the creep behavior of the material under constrained conditions. The 2D axisymmetric analysis, due to geometrical and loading symmetry, was carried out using quadrilateral elements with

ABAQUS 6.10 FE solver, Figure 2(a). The nodes along AB were restrained in the Y-direction and the nodes along AD were restrained in the X-direction. The uniform stress was applied on face CD. Norton's creep law ($\dot{\epsilon}_s = A\sigma^n$) relating the steady state creep rate ($\dot{\epsilon}_s$) with applied stress (σ) was used as a constitutive equation for the analysis. In the analysis, the elastic modulus was assumed to be 200 GPa, and constant A in the Norton's equation was selected to give a steady state creep rate of 10^{-5} h^{-1} at 200 MPa for a given value of stress exponent n . The calculations were carried out for the n values ranging from 1 to 10. A similar approach was adopted earlier to estimate stress distribution across a constrained specimen.^[21] Initially, the material was assumed to deform elastically followed by creep deformation. A typical mesh used in FE analysis is shown in Figure 2(b). The stresses were calculated in all the three directions, viz., radial (S_{xx}), axial (S_{yy}), and hoop (S_{zz}), as shown in Figure 2(c). The element size was reduced closer to the notch root, and elastic analysis was used to assure that the mesh configuration was sufficiently

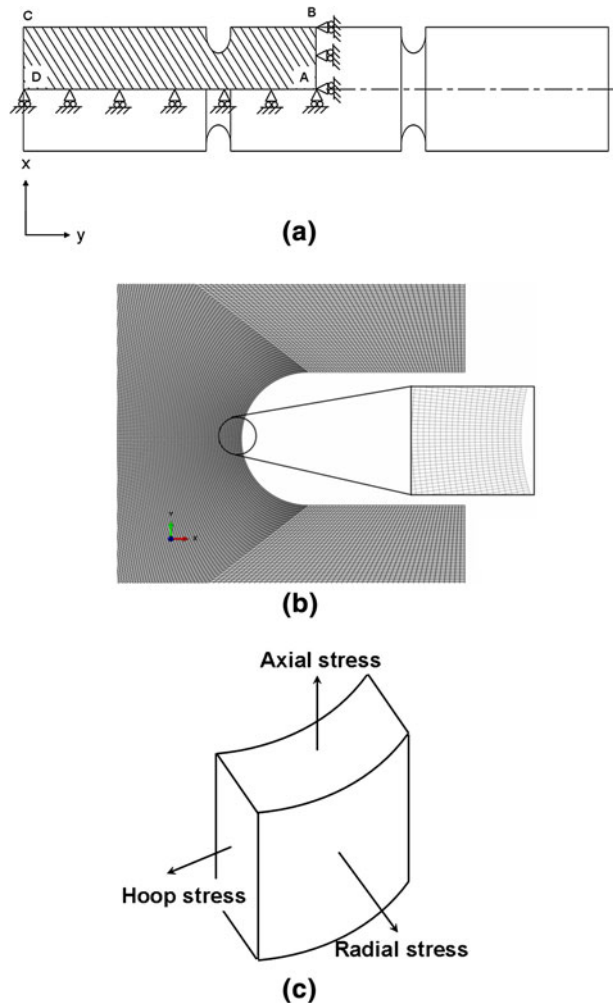


Fig. 2—Schematic of (a) notched specimen depicting the meshed area and boundary conditions, (b) the finite element mesh used in the analysis of stress distribution across the notch throat plane (notch acuity ratio = 10), and (c) direction of stresses in notched specimens.

refined near the notch root for the theoretical stress concentration factor.^[27] The analysis was continued till the stress redistribution across the notch throat plane attained a stationary state condition. The stress redistribution was generally considered to attain stationary state condition when the total strain at the notch throat plane reached the elastic strain in the material as stated by Calladine.^[28]

C. Governing Equations for Creep Damage Evolution

The estimation of creep damage evolution in the material under uniaxial as well as triaxial state of stress imposed by the constraint (notch) necessitates the inclusion of the tertiary stage of creep deformation in the material model. CDM, proposed by Kachanov,^[29] has been widely accepted for prediction of the tertiary stage of creep behavior of the materials and is used in this investigation to estimate the creep damage across the notch plane.

The creep deformation rate of the material under triaxial state of stress can be defined by^[13]

$$\dot{\epsilon}_{cij} = \frac{3}{2} A \left(\frac{\sigma_{vm}}{1-\omega} \right)^{n-1} \frac{\sigma'_{ij}}{1-\omega}, \quad [1]$$

where A and n are coefficients in Norton's law, σ_{vm} is the von-Mises stress, σ'_{ij} is the deviatoric stress component, and ω is the damage parameter varying from 0 to 1 indicating virgin material and fully damaged material, respectively. The creep damage rate as a function of representative stress and current damage is given by

$$\dot{\omega} = \frac{B\sigma_{rep}^\chi}{(1-\omega)^\phi}, \quad [2]$$

where B , ϕ , and χ are material constants and σ_{rep} is the representative stress^[27] and is defined by

$$\sigma_{rep} = \alpha\sigma_1 + (1-\alpha)\sigma_{vm}, \quad [3]$$

where α is the material constant and σ_1 and σ_{vm} are the maximum principal stress and von-Mises stress, respectively.

The creep strain rate (Eq. [1]) and damage rate (Eq. [2]) equations under uniaxial stress (unconstrained condition) converge to the following expressions, respectively,^[13]

$$\dot{\epsilon}_c = A \left(\frac{\sigma}{1-\omega} \right)^n. \quad [4]$$

$$\dot{\omega} = \frac{B\sigma^\chi}{(1-\omega)^\phi}. \quad [5]$$

In order to predict the creep life of the plain specimen, B and ϕ coefficients of creep damage (Eq. [5]) were obtained by a trial and error method considering the good fit of estimated creep curve and rupture life with those of the experimentally obtained values. The values of material constants used in the analysis are given in Table III.

Table III. Creep and Damage Constants for 9Cr-1Mo Steel at 873 K (600 °C)

E (MPa)	ν	A	n	χ	ϕ	B
160,000	0.3	1.272×10^{-21}	8.34	8.24	10.0	2.076×10^{-21}

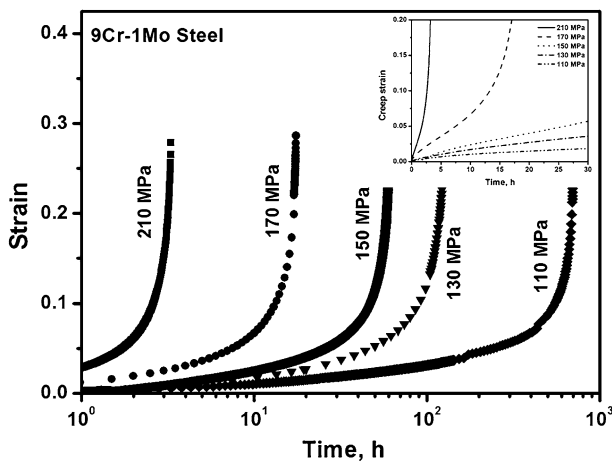


Fig. 3—Variation of creep strain as a function of time, creep tested at different stresses under uniaxial creep loading at 873 K (600 °C).

Eqs. [1] and [2] have been used in predicting creep deformation and rupture behavior of the material under triaxial state of stress employing ABAQUS FE solver. A user material subroutine VUMAT has been written for calculating the stresses, creep strains, damage, and rupture life of the notched specimen.

III. RESULTS AND DISCUSSION

A. Creep Behavior of the Steel Under Unconstrained Condition

Creep tests were carried out on the plain specimen at 873 K (600 °C) over a uniaxial stress range of 110 to 210 MPa. The variations of creep strain with time at different stresses are shown in Figure 3. Creep deformation of the steel was characterized by a small instantaneous strain on loading, a transient primary stage, and a secondary stage, followed by prolonged tertiary creep regime. A short transient and a prolonged tertiary stage indicated that the strain hardening in the material rapidly recovered at such a high homologous temperature. In normalized and tempered ferritic-martensitic steels, the occurrence of transient creep has been reported to be the consequence of movement and annihilation of high dislocation density, which are introduced in the material during martensite transformation on normalization heat treatment.^[30] Loss of creep strength due to the microstructural instability of the material on creep exposure is considered as the main cause of early onset of the tertiary stage during creep deformation.^[30] A variation of steady state creep rate ($\dot{\epsilon}_s$) with applied stress (σ) of the material is shown in Figure 4. The variation followed Norton's law, a power

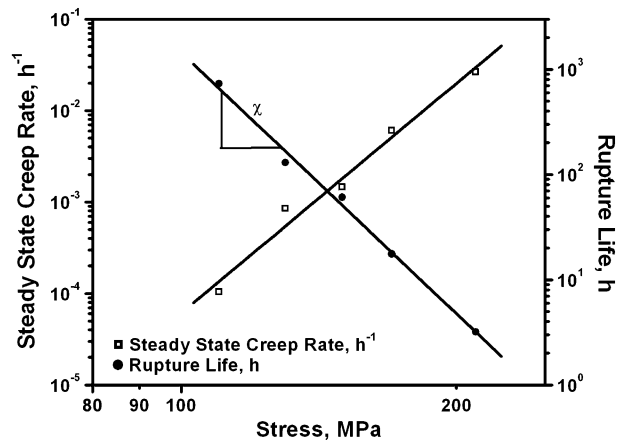


Fig. 4—Variations of steady state creep rate and rupture life as a function of applied stress for plain specimens.

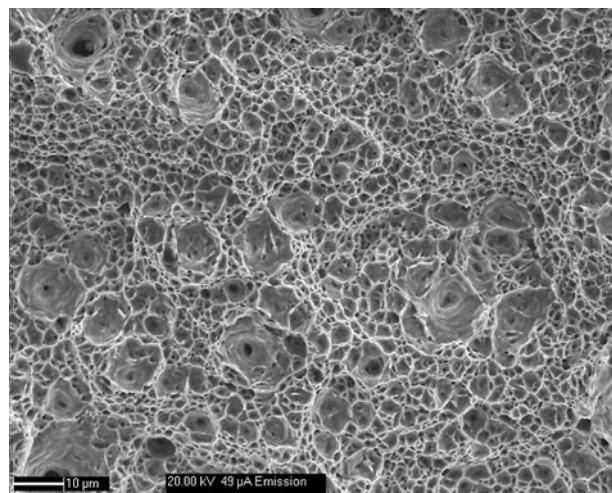


Fig. 5—Transgranular dimpled fracture of plain specimen, creep tested at 150 MPa, 873 K (600 °C).

law relation of the form, $\dot{\epsilon}_s = A\sigma^n$, where A is a constant and n is the stress exponent. The creep mechanism expected in this stress and temperature range is climb control dislocation creep as depicted by the value of stress exponent n as 8.34. The variation of rupture life (t_r) of the 9Cr-1Mo steel with applied stress (σ) is shown in a double-logarithmic plot in Figure 4. Rupture life was found to decrease with increase in applied stress and obeyed a power law relation as $t_r = M\sigma^{-m}$, where M and m are the stress coefficient and the stress exponent, respectively. The value of m was found to be 8.24. The creep deformation rate and rupture life are related to the Monkman–Grant relation.^[31] The absolute values of n (relating creep deformation to stress) and m (relating rupture life to stress) were close to each other, indicating that the same mechanism would be operating for deformation and fracture. SEM examination of the fracture surface of the creep ruptured plain specimen tested at 150 MPa and 873 K (600 °C) revealed a ductile transgranular fracture characterized by a dimple appearance (Figure 5), resulting from the

coalescence of intragranular microvoids. Similar observations on the fracture surface appearance in specimens creep tested at all applied stresses indicate the absence of creep cavitation in this steel under uniaxial loading. Transgranular ductile dimple fracture appearance in forged 9Cr-1Mo steel ruptured under creep conditions has also been reported by Choudhary *et al.*^[31]

The time to onset of the tertiary stage of creep deformation, “ t_{ot} ,” was estimated from the creep curves. The time to onset of the tertiary stage was measured from the variation of creep rate with time at which the creep rate attained its minimum and beyond which the creep rate accelerated. The variation of “ t_{ot} ” with rupture life is shown in Figure 6. It followed a linear equation of the form $t_{ot} = f \times t_r$, where f is a constant. The constant f was found to be around 0.52, which suggests that the steel spent about 48 pct of its creep life in the tertiary stage of deformation. Investigations carried out by Choudhary *et al.*^[31] on 9Cr-1Mo steel have reported the value of f as low as 0.32 with a decrease in applied stress. The extensive tertiary stage of creep deformation in terms of both the time spent and accumulation of creep strain observed in this steel is in agreement with the behavior of other grades of tempered martensitic ferritic steels.^[32] Based on the CDM approach, an indication of the damage process initiating the tertiary stage of creep deformation is provided by the creep damage tolerance parameter defined as $\lambda = \epsilon_f / (\dot{\epsilon}_s \cdot t_r)$, where ϵ_f is strain to failure, $\dot{\epsilon}_s$ is steady state creep strain rate, and t_r is rupture life.^[33–35] The onset of the tertiary stage of creep deformation is attributed to different damage mechanisms such as microstructural degradation, intergranular creep cavitation, mechanical instability, *etc.* Each damage micromechanism, when acting alone, results in a characteristic shape of the creep curve and a corresponding characteristic value of λ .^[33–35] The materials which are microstructurally stable and display only a limited tertiary stage of creep deformation due to intergranular creep cavitation exhibit $\lambda < 2$, whereas the materials which are microstructurally unstable during creep exposure exhibit $\lambda > 2$. Figure 7 shows the variation of creep damage tolerance factor λ with rupture time. The value

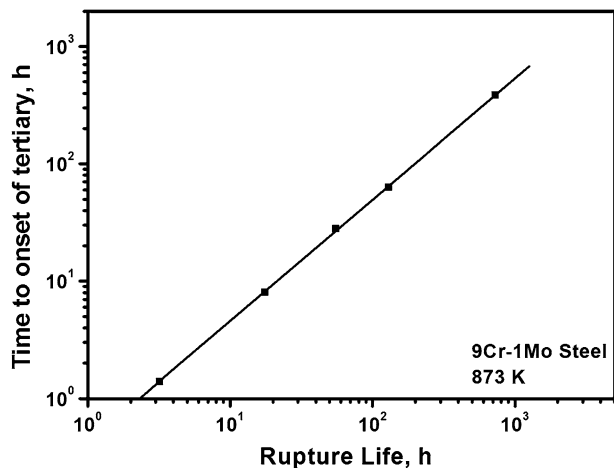


Fig. 6—Variation of time to onset of tertiary creep (t_{ot}) as a function of rupture life of plain specimen.

of λ was found to be around 4.2 for the investigated steel and was almost independent of rupture life. Such a high value of λ indicates the coarsening of precipitates, dislocation substructures, and martensitic lath as the dominant damage mechanisms operating in the steel during creep exposure.^[34]

B. Creep Behavior of the Steel Under Constrained Condition

1. Effect of net applied stress

The creep rupture lives of the steel under constrained condition, imposed by incorporating a notch of root radius 1.25 mm in the smooth specimen, were found to be higher than that of the unconstrained specimens for all the investigated stresses (Figure 8), exhibiting creep strengthening in the presence of constraint. Nominal stress (net stress) at the notch throat was considered as applied stress for a notched specimen. The strengthening effect (ratio of rupture life of notched specimen to plain

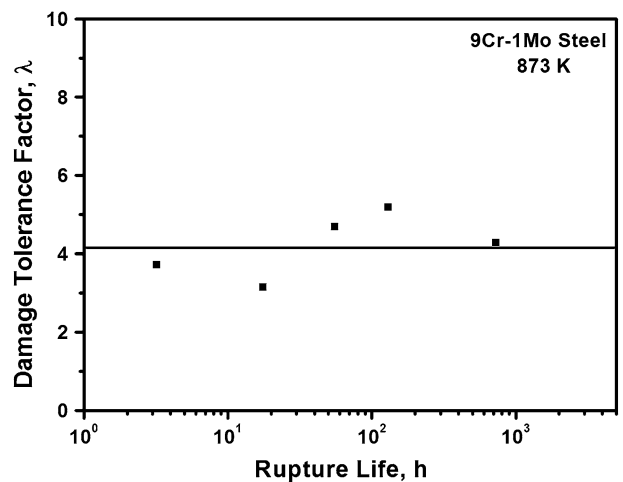


Fig. 7—Variation of damage tolerance factor as a function of rupture life for plain specimen.

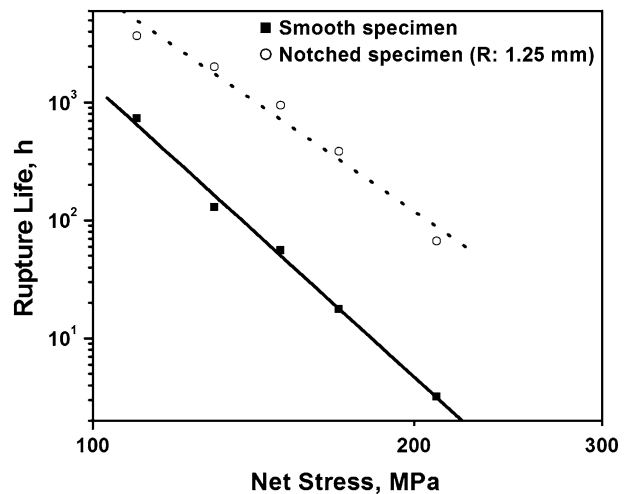


Fig. 8—Variations of rupture lives of plain and notched specimens as a function of net applied stress.

specimen) increased with the increase in applied stress, Figure 9. However, at relatively lower applied stresses, as in the case of the plant operating conditions, the creep cavitation would be predominant, leading to notch weakening. As in the plain specimen, the rupture life of a notch specimen decreased with increase in applied stress and obeyed a power law relation as $t_r = M'\sigma^{-m'}$, where M' and m' are the stress coefficient and the stress exponent, respectively (Figure 8). The value of m' under notched conditions was found to be 6.24. The applicability of the Monkman–Grant relationship for notched specimens has been justified by Lukas *et al.*^[36] Based on the Monkman–Grant relation, the absolute value of n for a notched specimen is expected to be around 6.24. This indicates that the climb-controlled dislocation creep mechanism would also be operating in notched specimens. Under constrained creep condition, the values of stress exponent and stress coefficient were found to decrease. The pct reduction in area of the steel

with rupture life under constraint is shown in Figure 10. Under constrained conditions, creep rupture ductility of the steel decreased significantly with rupture life compared to that in the unconstrained condition.

SEM fractograph of the notched specimen creep tested at 150 MPa is shown in Figure 11. The fracture surface with a dimple appearance indicated the transgranular ductile failure, Figure 11(a). Shear lip failure caused by the final mechanical instability at the notch root was observed, Figure 11(b), resulting in a cup-and-cone type of failure appearance. This indicated that the failure began at the central location of the notched specimen and propagated toward the notch root. The width of the shear lip zone was found to decrease with a decrease in applied stress. The shape and size of the dimples in the failed notched specimens were found to depend on the applied stress. In general, the dimples became shallower and bigger in size with a decrease in applied stress.

2. Effect of degree of constraint

The degree of constraint to creep deformation had been varied by varying the root radius of the notch from 0.25 to 5 mm in the specimen. Creep rupture tests were

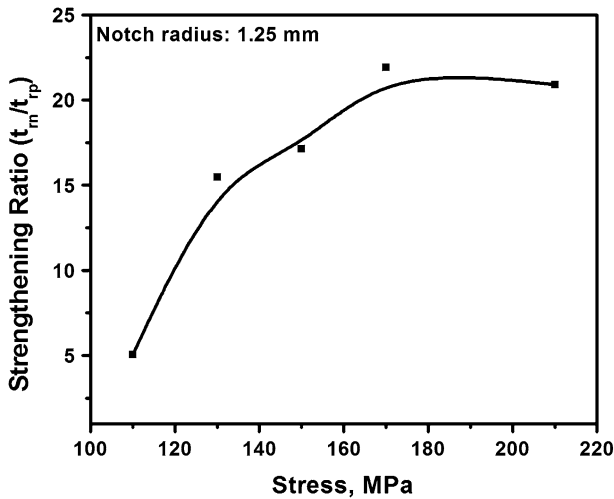


Fig. 9—Variation of strengthening ratio, defined as rupture life of notched specimen to rupture life of plain specimen, with net applied stress for notch specimen of root radius 1.25 mm.

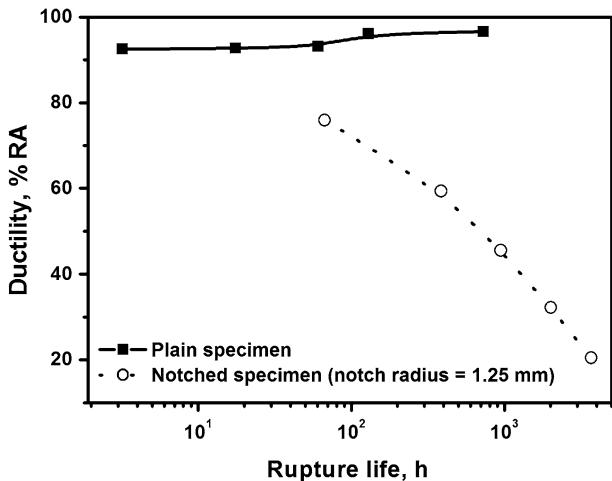


Fig. 10—Variation of rupture ductility [pct reduction in area (RA)] of plain and notch specimens as a function of rupture life.

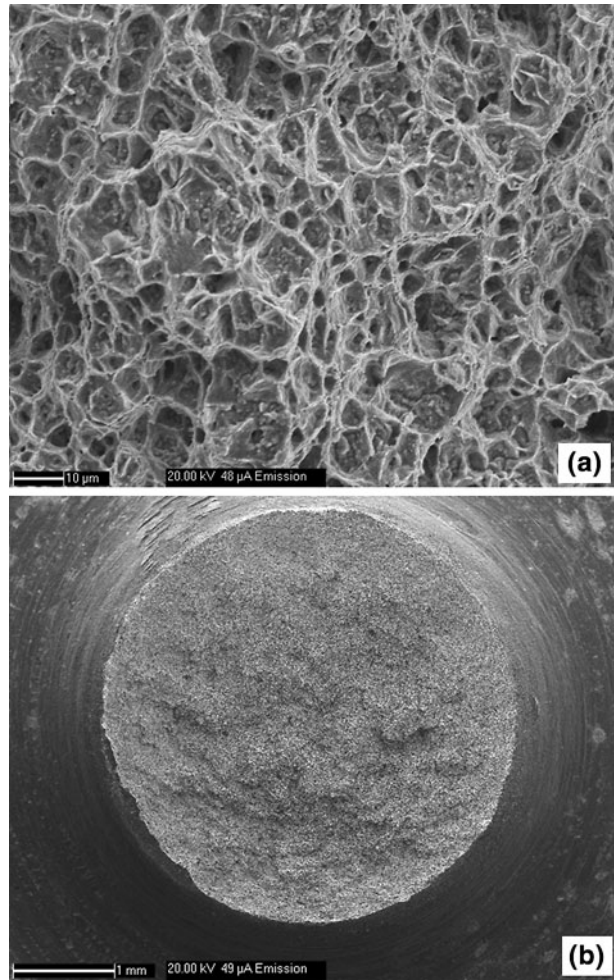


Fig. 11—(a) Transgranular dimple failure observed in notched specimen and (b) cup-and-cone type fracture (notch root radius = 1.25 mm), 150 MPa and 873 K (600 °C).

carried out at 150 MPa and 873 K (600 °C). The rupture life was found to increase rapidly with increase in notch acuity (constraint) and tended to saturate at a higher notch acuity ratio (Figure 12). The creep rupture ductility (pct reduction in area) of the steel decreased significantly with an increase in notch acuity ratio and became almost invariant at a higher notch acuity ratio (Figure 13). SEM macrofractography of the creep ruptured notched specimens having a notch root radius of 2.5 and 0.25 mm, creep tested at 150 MPa, 873 K (600 °C), are shown in Figures 14(a) and (b), respectively. Shear lip, resulting from the cup-and-cone type of ductile failure, caused by the final mechanical instability at the notch root, was observed for the relatively shallow notches (less constraint), Figure 14(a), whereas predominantly brittle failure with significantly less reduction in ductility was observed for specimens having relatively sharper notches with a high acuity ratio, Figure 14(b). SEM fractographs at the central and notch root location

of the creep fractured notched specimen of a notch root radius of 0.25 mm are shown in Figures 15(a) and (b), respectively. Predominantly intergranular creep failure was observed around the notch root location, Figure 15(b). Metallographic investigation of the unfailed notch of the creep ruptured specimen revealed extensive intergranular creep cavitation close to the notch root, Figure 15(c). Mechanical instability around the central location of the notch, as evident by transgranular ductile fracture with a dimple appearance (Figure 15(a)), caused the final failure of the notch specimen having relatively sharper notches. The proportion of intergranular creep failure appearance in the fracture surface increased with an increase in degree of constraint.

C. Analysis of Stress Redistribution Under Constrained Condition

Stress redistribution across the notch throat plane during creep exposure has been reported by several investigators.^[7,8] In this investigation, FE analysis of stress distribution across the notch throat plane of the

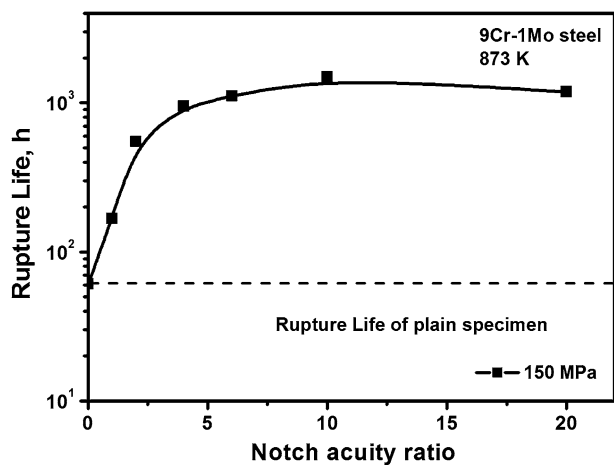


Fig. 12—Variation of creep rupture life of notched specimen as a function of notch acuity ratio creep tested at 150 MPa and 873 K (600 °C).

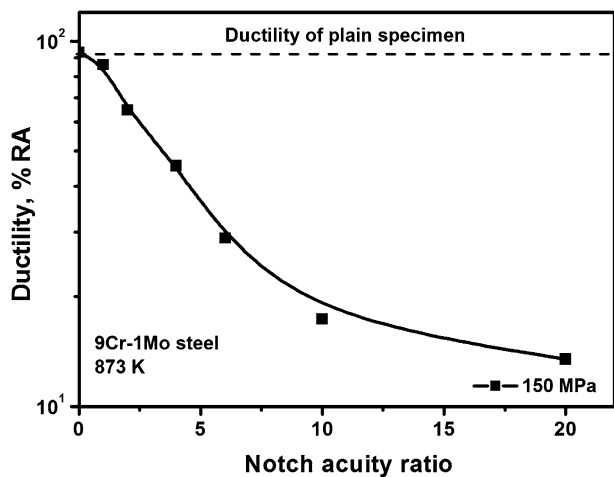


Fig. 13—Variation of creep rupture ductility of notched specimen as a function of notch acuity ratio, creep tested at 150 MPa and 873 K (600 °C).

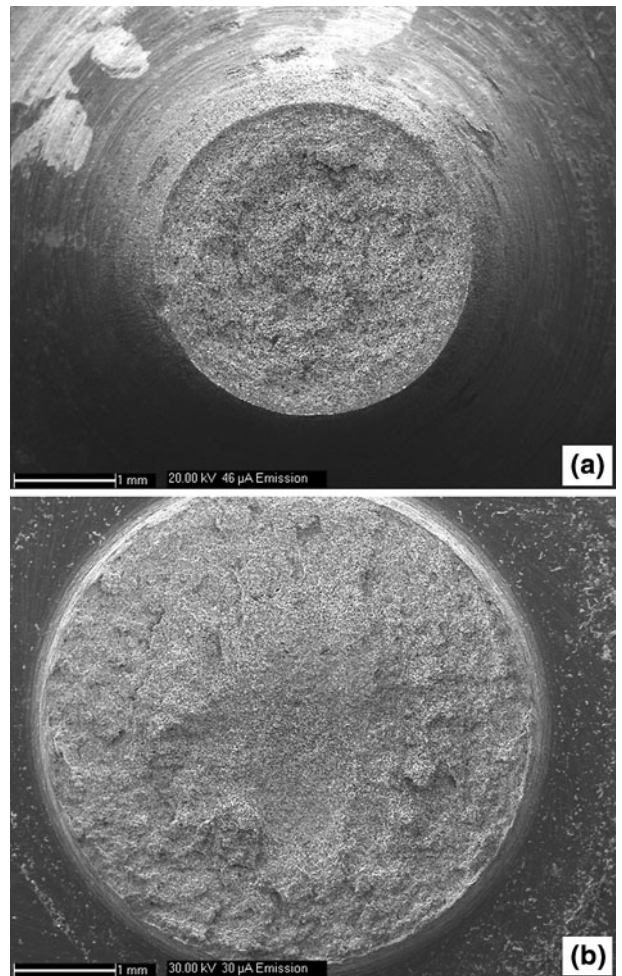


Fig. 14—SEM micrographs: (a) Typical cup-and-cone fracture with shear lip observed in notched specimen at relative shallow notches (notch radius of 2.5 mm) and (b) mixed mode fracture for relatively sharper notches (notch radius of 0.25 mm) at 150 MPa, 873 K (600 °C).

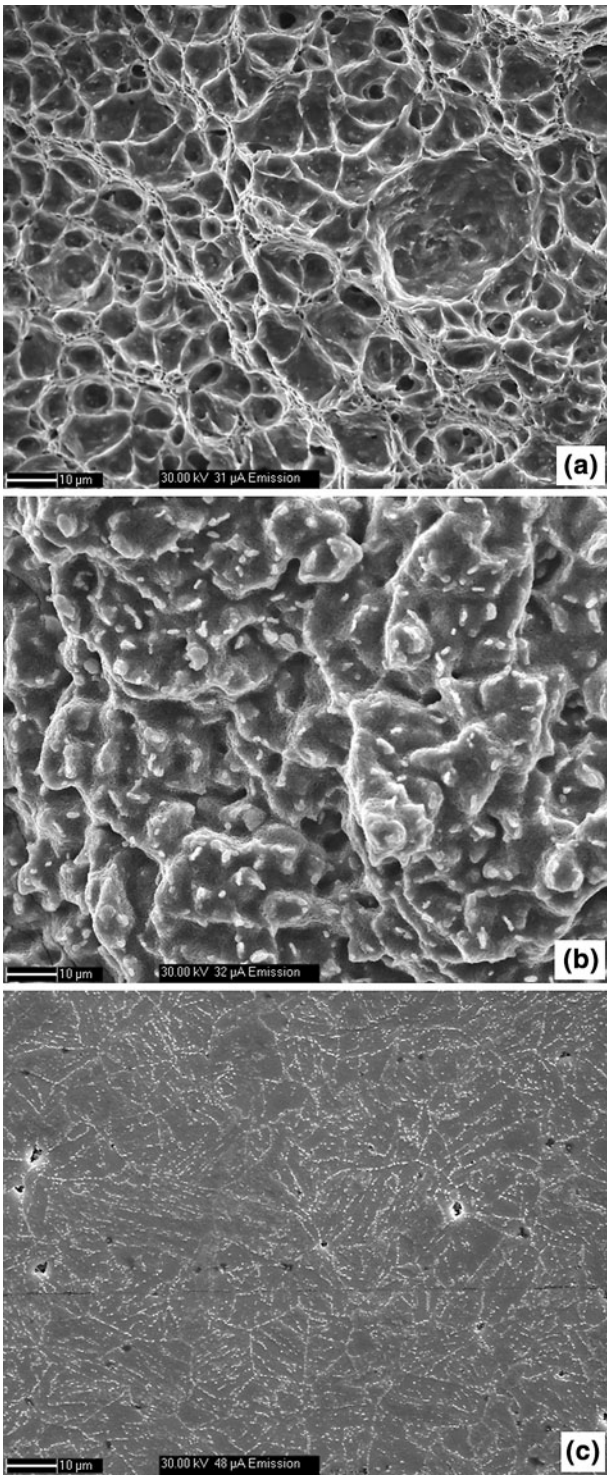


Fig. 15—SEM micrographs: (a) Ductile transgranular fracture at central region, (b) brittle intergranular fracture associated with (c) creep cavitation at notch root for relatively sharper notches (notch radius of 0.25 mm) at 150 MPa, 873 K (600 °C).

9Cr-1Mo steel was carried out. The analysis consisted of two steps, *viz.*, elastic deformation immediately after the loading and subsequent creep deformation. The variations of normalized radial, axial, and hoop stresses across the notch plane for different fractions of time to reach a stationary state, for the notch of root radius of

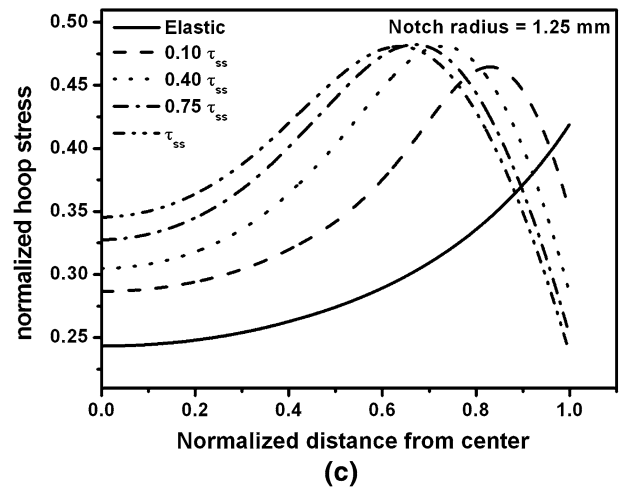
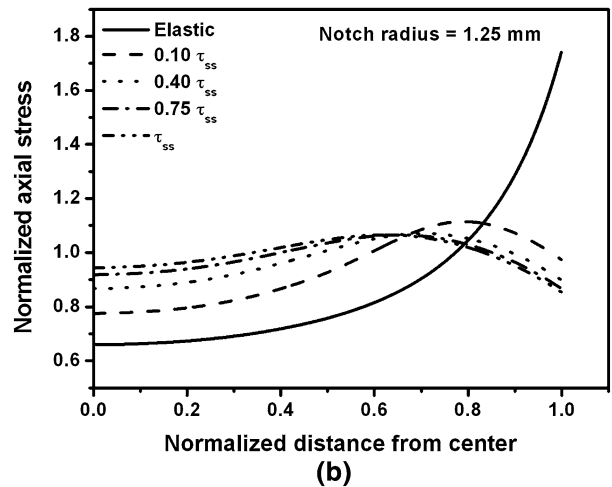
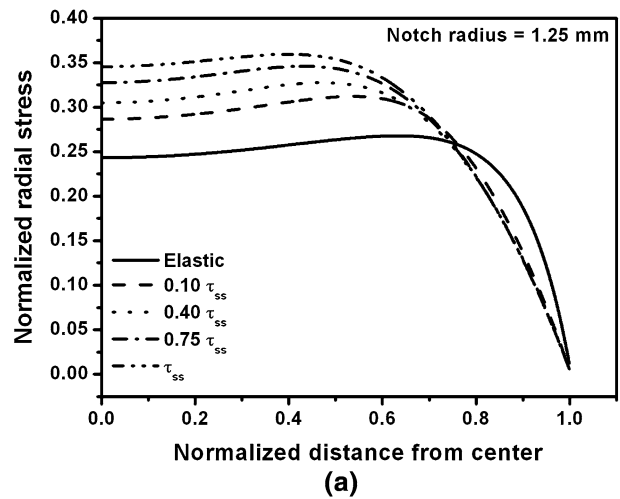


Fig. 16—Redistribution of normalized stresses across notch plane for notch radius of 1.25 mm, (a) radial stress, (b) axial stress, and (c) hoop stress for the stress exponent (n) of 7.

1.25 mm and for stress exponent (n) of 7, are shown in Figure 16. The stresses were normalized with respect to the net applied stress. The radial stress that arose from elastic deformation was found to be significantly lower than that of net applied stress (Figure 16(a)). The stress

was higher at the central region of the notch plane and decreased toward the notch root. The stress redistribution during creep exposure led to an increase in the radial stress. The axial stress was found to be significantly higher at the notch root than that around the center of the notch plane after elastic deformation (Figure 16(b)). With creep exposure, the axial stress at the center of the notch plane increased, whereas it decreased at the notch root. The stationary state distribution of axial stress showed a maximum close to the notch root and had a value higher than the net applied stress. After elastic deformation, the hoop stress was significantly lower than the net applied stress (Figure 16(c)). With creep exposure, the hoop stress increased around the central region of the notch and decreased at the notch root. The hoop stress exhibited maxima similar to axial stress after attaining the stationary state and had a value lower than the net applied stress.

D. Creep Cavitation and Stress State

Creep cavitation in materials proceeds with the nucleation of creep cavities and their growth followed by linkage into discrete cracks, leading to failure. Nucleation of creep cavity in Cr-Mo ferritic steels under constrained conditions has been discussed by Cane,^[9] Goyal *et al.*,^[37] and Perrin and Hayhurst.^[38] Nucleation of creep cavity is associated with the stress concentration around the grain boundary irregularities like grain boundary triple point, ledges, particles, *etc.*, which is produced by inhomogeneous plastic deformation around them. Since the shear stress is required for the plastic deformation to occur, von-Mises stress plays a major role in creep cavity nucleation.^[19] However, stability of the nucleated creep cavities is decided by the maximum principal stress as the critical cavity size r_c which can avoid the sintering is governed by $r_c = 2\gamma_c/\sigma_1$, where γ_c is the surface energy and σ_1 is the maximum principal stress. For the growth of existing creep cavity, it has to attain the critical size, otherwise the cavity will sinter. The nucleated stable creep cavity can grow basically by two mechanisms: (i) plasticity-controlled growth^[37,39,40] and (ii) stress-directed flow of atoms (diffusive growth).^[41] Cavity growth by plasticity occurs as a result of creep deformation of the matrix surrounding the grain boundary cavity in the absence of vacancy flux.^[42] The von-Mises stress will assist the cavity growth by inducing plasticity, whereas cavity growth by stress-directed flow of the atom will be controlled by maximum principal stress. The cavity growth at high temperatures can also be driven by the hydrostatic component of the stress state, as in the case of high temperature ductile fracture.

Since creep deformation and rupture behavior of the material under constrained conditions depend on the von-Mises, principal, and hydrostatic stresses, these stresses in stationary state conditions were calculated from the FE-estimated stationary state radial, axial, and hoop stresses (Figure 17). The variations of the normalized stationary state von-Mises stress across the notch throat plane for different notch acuity ratios are shown

in Figure 17(a). The von-Mises stress remained below the net applied stress and was almost uniform across the notch plane in the case of relatively shallow notches. With an increase in notch sharpness (notch acuity ratio),

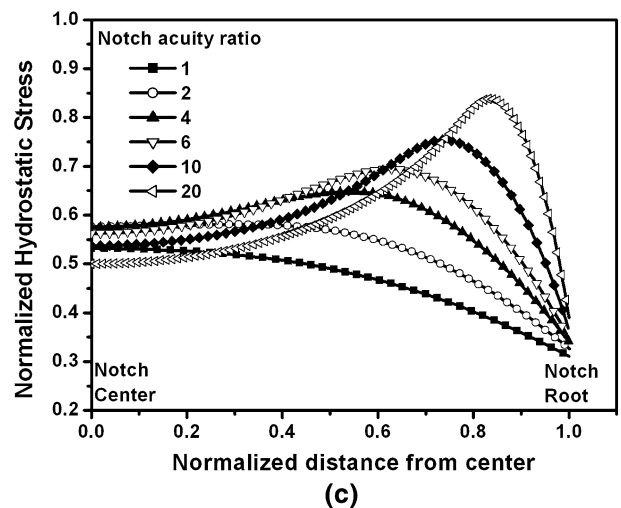
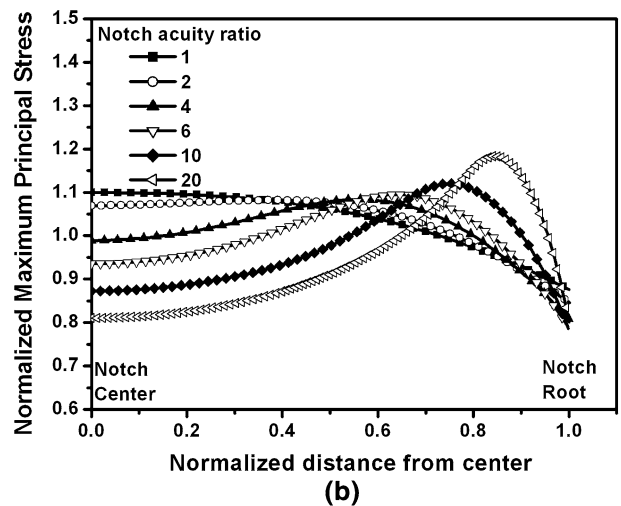
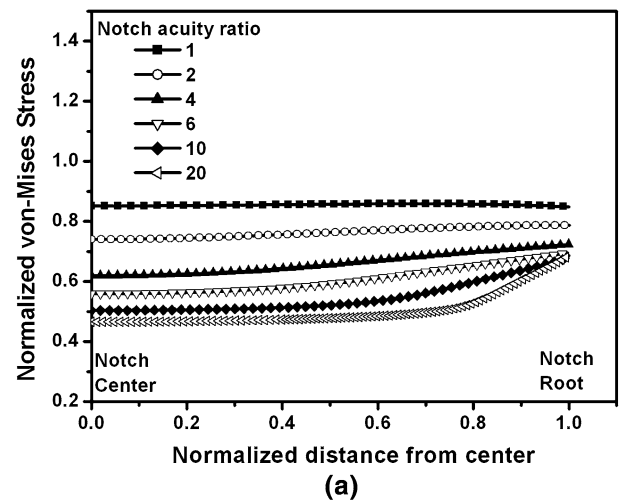


Fig. 17—Variations of stationary state normalized (a) von-Mises, (b) maximum principal, and (c) hydrostatic stress across the notch plane as a function of degree of constraint (stress exponent = 10).

the von-Mises stress decreased more at the central location of the notch throat plane than near the notch root, leading to higher stress at the notch root than that at the notch central region. The variation of normalized stationary state maximum principal stress across the notch plane for different notch acuity ratios is shown in Figure 17(b). The principal stress variation showed a maximum value which was more than the net applied stress, and it increased and shifted toward the notch root with notch sharpness. The behavior of hydrostatic stress under stationary state conditions across the notch plane for different notch acuity ratios (Figure 17(c)) was similar to that of the principal stress, but the maximum value of the hydrostatic stress remained below the net stress for all the notch acuity ratios investigated.

As the nucleation of creep cavities is controlled by von-Mises stress through plastic deformation, nucleation of creep cavities is expected to be more in the notch root region for relatively sharper notches (Figure 17(a)). High principal stress along with high hydrostatic stress for relatively sharper notches (Figures 17(b) and (c)) would have led to the growth of the nucleated cavities at the near notch root region (Figure 15(c)). The fracture surface appearance near the notch root is expected to be intergranular as observed (Figure 15(b)). Coalescence of the creep cavities would have led to the propagation of the crack from the notch root region toward the central region of the notch throat plane. Final failure of the ligament at the central region of notch plane would have occurred due to mechanical instability resulting in ductile dimple fracture appearance at the notch central region (Figure 11(a)).

The factors that influence the creep fracture behavior of the material under constrained conditions as in the notched specimen had been studied by Wu *et al.*^[7] The factors are maximum principal stress and its location, strain at notch root, local *vs* global events, hydrostatic stress, and stress triaxiality factor. Among them, the most relevant factor was the stress triaxiality. The triaxiality factor (TF) has been defined as^[7]

$$TF = \frac{\sigma_m}{\sigma_{vm}} = \left(\frac{\sigma_1 + \sigma_2 + \sigma_3}{3} \right) \frac{1}{\sigma_{vm}}. \quad [6]$$

The distribution of TF across the notch throat for notch acuity ratio of 4 and 20 is shown in Figures 18(a) and (b), respectively. The triaxiality was found to be maximum at the central location of the notch plane for the relatively shallow notches. The magnitude of the maximum value of TF increased and the location shifted toward notch root with an increase in sharpness of the notch (high constrained notches). If triaxiality is assumed to be the most important indicator of constraint deformation, then the fracture surface appearance indicated a higher void nucleation and growth near the central region of the notch for the relatively shallow notches (Figure 15(a)) and creep cavitation-induced brittle fracture near the notch root for the relatively sharper notch (Figure 15(b)) by enhancing the creep cavity growth. Similar experimental observations are reported by Dyson and Loveday^[2] in Nimonic 80 and Al-Abed *et al.*^[17] in

2.25Cr-1Mo steel under multiaxial state of stress. Hancock^[43] indicated that the failure process in notched specimens is the competitive process between plastic strain and high triaxiality levels at different locations of the notch plane. In the present study, plastic strain controlled by von-Mises stress is the dominant factor governing the creep rupture strength of the steel under constrained conditions, as stated in subsequent sections.

E. Estimation of Creep Rupture Life

1. Unconstrained condition

Analysis of creep damage was carried out using ABAQUS FE solver for the notched specimen. The creep damage law was incorporated using VUMAT subroutine using the Eqs. [1] through [3]. A user material subroutine VUMAT was written in FORTRAN and implemented in the ABAQUS Explicit for calculating the stresses, creep strains, and damage in the plain and notched specimens. In order to predict the creep rupture life of the plain specimen, *B* and ϕ coefficients of creep damage (Eq. [2]) were obtained by the trial and error method considering the good fit of estimated life using Eq. [3] with the experimental values. The values of material constants used in the analysis are given in Table III. VSPRINC utility subroutine was used for calculating the maximum principal stress at each integration point which was used for estimating representative stress. The rate equations for creep strain (Eq. [1])

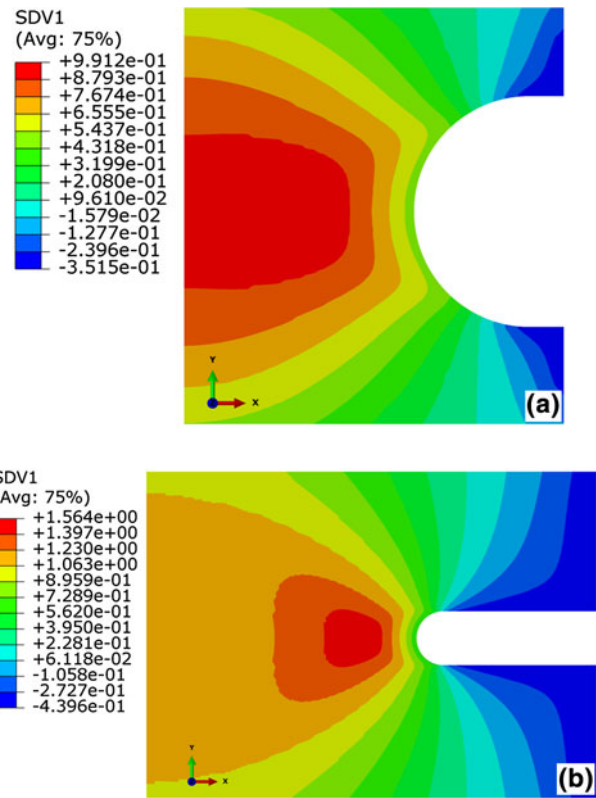


Fig. 18—Distribution of triaxiality factor across the notch (a) for relatively shallow (notch root radius = 1.25 mm) and (b) sharper notches (notch root radius = 0.25 mm).

and damage (Eq. [2]) were solved and the increment of the variables was calculated, and at the end of increment all the variables were updated within the VUMAT subroutine and passed on to main program. The value of damage parameter was chosen to be 0.5. As the damage parameter increased beyond this value, the accelerated creep rate led to severe distortion of the elements.

The comparison of creep curves of the plain specimens estimated from CDM (Eq. [4]), FE analysis, and experimentally obtained creep curves is shown in Figure 19. The predicted creep curves were found to be in good agreement with the experimental creep curves. Figure 20 shows the comparison between experimental and predicted creep rupture life for the plain specimen. The predicted creep rupture life was found to be in good agreement with the experimentally observed creep rupture life within a factor of around 1.5.

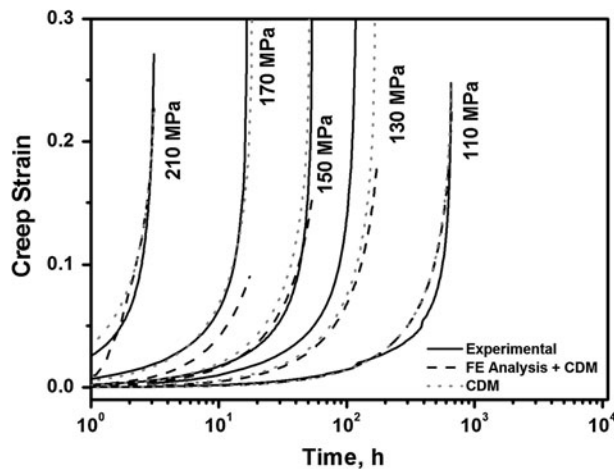


Fig. 19—Prediction of creep curves of plain specimens at various applied stresses at 873 K (600 °C).

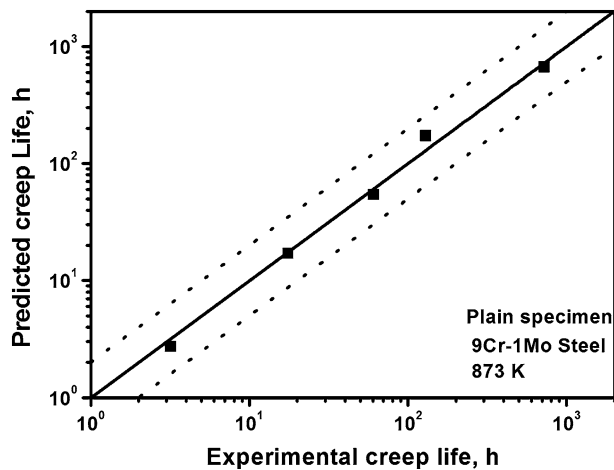


Fig. 20—Prediction of creep rupture life of plain specimens at various applied stresses at 873 K (600 °C).

2. Constrained condition

The stress–creep rupture life relation under the triaxial state of stress has been expressed based on representative stress defined as

$$t_r = M\sigma_{rep}^{-m}. \quad [7]$$

The representative stress, σ_{rep} , is defined as the stress which gives rise to the same creep rupture life for the uniaxial plain specimen as the notched bar specimen. A notched specimen is said to be notch strengthening if $\sigma_{rep} > \sigma_{net}$ and notch weakening if $\sigma_{rep} < \sigma_{net}$. This stress under a triaxial state of stress is generally defined by a combination of maximum principal stress and von-Mises stress. Since the stresses vary across the notch plane during creep exposure and attain the stationary states as discussed in Section III–C (Figure 17), it is difficult to identify the location in notch plane where the stresses can be considered in defining the representative stress. Webster *et al.* and Hayhurst and Webster,^[11,21] based on FE analysis, had introduced the skeletal point concept in determining the representative stress. The skeletal point is the location in the notch plane for a given notch geometry, where the variation of stress across the notch plane for different stress exponents n in Norton’s law intersects. The variation of principal stress across the notch throat for various values of stress exponent n showed that they pass through a skeletal point (Figure 21). The stresses at this point have been used to characterize the creep deformation, damage, and failure behavior of the material under triaxial state of stress. Figure 22 shows the variation of skeletal point maximum principle, von-Mises, and hydrostatic stresses with notch acuity ratio. The maximum principal and hydrostatic stresses at the skeletal point increased with notch acuity ratio and tend to saturate at a higher notch acuity ratio, whereas von-Mises stress decreased with an increase in notch acuity ratio. The value of maximum principal stress at the skeletal point was more than the net stress. However, von-Mises and hydrostatic stress at

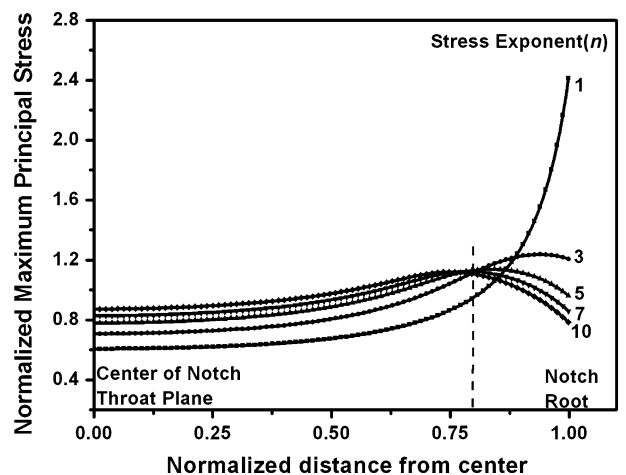


Fig. 21—Variation of stationary state maximum principal stress across the notch plane for notch root radius of 0.5 mm and different values of stress exponent n , showing skeletal point.

the skeletal point were lower than the net stress for all the notch acuity ratios.

Having considered the skeletal point stresses governing the creep rupture life of the steel under constrained condition, the α value in the representative stress $\sigma_{rep} = \alpha\sigma_1 + (1 - \alpha)\sigma_{vm}$ was estimated from the regression analysis using the skeletal point stresses. The best fit value of α was found out to be 0.06. The creep rupture life of the steel under multiaxial state of stress is considered to be governed predominantly by von-Mises stress with only 6 pct maximum principal stress (Figure 23). To predict the rupture life of the steel under constrained condition, the representative stress was calculated within the VUMAT subroutine at each integration point during increment using von-Mises stress and maximum principal stress. The rupture life predicted based on the CDM coupled with FE analysis was found to be in good agreement with the experiments, Figure 24. The accuracy

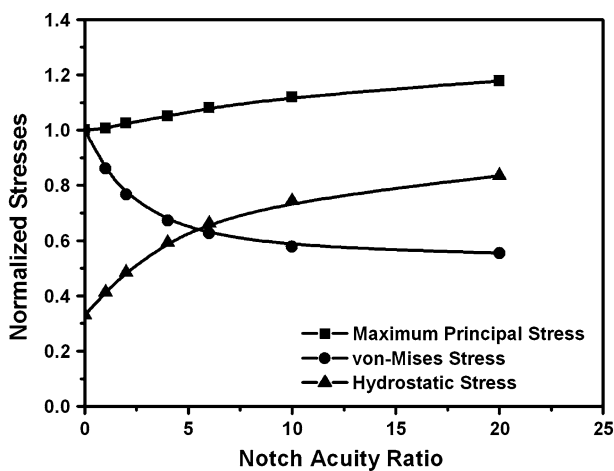


Fig. 22—Variations of normalized maximum principal, von-Mises, and hydrostatic stresses at skeletal point, as a function of notch acuity ratio.

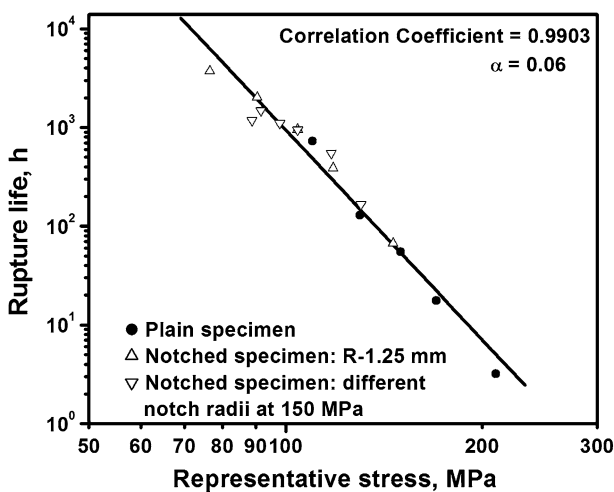


Fig. 23—Variation of creep rupture lives of plain and notch specimens with representative stress $[(\sigma_{rep} = \alpha\sigma_1 + (1 - \alpha)\sigma_{vm})]$ with $\alpha = 0.06$.

of prediction of creep rupture life in the notched specimens is slightly poor compared to the uniaxial specimens. The predictions of creep rupture life in the present investigation are based on the skeletal point concept. However, in reality, the stresses vary significantly across the notch throat plane. This would lead to slight inaccuracy in prediction of rupture life of the notched specimens.

F. Creep Rupture Ductility Under Constrained Condition

The failure under constrained condition is associated with the creep cavity nucleation and their growth which depends on the distribution of stresses across the notch. The increase in hydrostatic stress leads to an apparent reduction in the ductility. A number of models have been proposed to account for this dependence and are generally based on the growth of a void in a deforming medium. These models show that the void growth rate is a function of the ratio between the hydrostatic stress (σ_m) and the von-Mises stress (σ_{vm}). This ratio, (σ_m/σ_{vm}), is often known as the triaxiality. The analytical work performed by McClintock^[40] and Rice and Tracey^[44] indicated the exponential increase in growth rate of microvoids with stress triaxiality in elastic-perfectly plastic materials. Cocks and Ashby^[45] carried out the approximate calculations of the grain boundary cavity growth rates of creeping material under triaxial state of stress and its effect on creep ductility. The model proposed by Rice and Tracey^[44] is based on hole growth by the rigid plastic deformation of surrounding matrix. The model proposed by Rice and Tracey^[44] and Cocks and Ashby^[45] can be represented by the following expressions, respectively:

$$\frac{\epsilon_f^*}{\epsilon_f} = \frac{0.521}{\sinh\left(\frac{3\sigma_m}{2\sigma_{vm}}\right)} \quad [8]$$

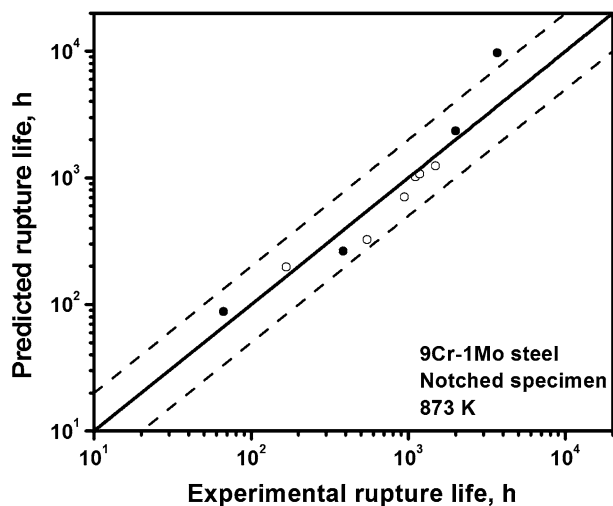


Fig. 24—Comparison of experimental creep rupture lives of notched specimens with those estimated by FE analysis, where solid circle data denote notch radius of 1.25 at various stress levels and open circle data, different constrained notches at 150 MPa.

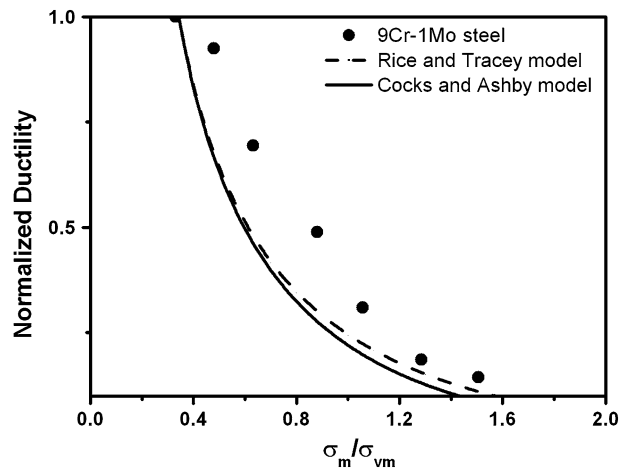


Fig. 25—Normalized rupture ductility as a function of ratio of hydrostatic/von-Mises stress based on Rice and Tracey^[44] and Cocks and Ashby^[45] models.

$$\frac{\varepsilon_f^*}{\varepsilon_f} = \sinh \left[\frac{2}{3} \left(\frac{n-1/2}{n+1/2} \right) \right] / \sinh \left[2 \left(\frac{n-1/2}{n+1/2} \right) \frac{\sigma_m}{\sigma_{vm}} \right], \quad [9]$$

where $\varepsilon_f^*/\varepsilon_f$ is the ratio of multiaxial to uniaxial creep ductility and n is the creep stress exponent.

Figure 25 shows the variation of normalized ductility (reduction in area pct) with the ratio of hydrostatic and von-Mises stress along with the prediction of creep ductility based on the Rice and Tracey^[44] and Cocks and Ashby^[45] models. Apparently, both the models were found to underestimate the creep ductility especially at higher notch acuity ratios. Enhanced oxidation of notch root region under strain during prolonged creep exposure (notch strengthening) might be a factor showing a higher reduction in area than those estimated by the models, and also the material is elasto-plastic not rigid plastic as assumed in the models.

IV. CONCLUSIONS

Based on the studies on creep deformation and rupture behavior of 9Cr-1Mo steel under unconstrained (plain) and constrained (notch) conditions and FE analysis of stress state across the notch coupled with CDM, the following conclusions have been drawn.

1. Under constrained conditions (incorporated by introducing a notch in the smooth cylindrical specimen), the creep rupture strength of the 9Cr-1Mo steel increased and the extent decreased with an increase in the degree of constraint and tended to saturate at a higher degree of constraint.
2. Plasticity-induced intragranular ductile failure with dimple appearance was observed for relatively low constrained conditions (shallow notches—lower notch acuity ratio). However, creep cavitation-induced intergranular brittle failure was observed for relatively high constrained conditions (sharper notches—higher notch acuity ratio). The creep damage was found to

initiate from the central location of the notch throat plane for shallow notches, whereas from the notch root for sharper notches.

3. The variations of maximum principal and hydrostatic stresses across the notch throat plane showed peak values which were higher than the net applied stress. The magnitude of the peak increased and the location shifted from the central location of the notch plane to close to the notch root with the increase in notch acuity ratio. The von-Mises stress decreased with an increase in notch acuity ratio and remained below the net applied stress.
4. The creep rupture life of the steel under constrained conditions has been predicted based on the FE analysis of the stress state across the notch coupled with CDM. A user material subroutine VUMAT has been written for calculating the stresses, creep strains, damage, and rupture life of the notched specimen.

ACKNOWLEDGMENTS

The authors are grateful to Dr. P.R. Vasudeva Rao, Director, Indira Gandhi Centre for Atomic Research (IGCAR), and Dr. T. Jayakumar, Director, Metallurgy and Materials Group, IGCAR, for their constant encouragement and support. The authors are also thankful to Dr. A.K. Bhaduri, Associate Director, Materials Development and Technology Group, IGCAR, for his keen interest in this work. The authors are grateful to Dr. C. Ravishankar, MTD, IGCAR, for the help rendered in FE analysis.

REFERENCES

1. D.R. Hayhurst: *J. Mech. Phys. Solids*, 1972, vol. 20, pp. 381–90.
2. B.F. Dyson and M. S. Loveday: in *Proc. Creep in Structures, IUTAM Symp.*, A.R.S. Ponter and D.R. Hayhurst, ed., Pergamon Press, Oxford, 1981, pp. 406–421.
3. K.D. Al-Faddagh, G.A. Webster, and B.F. Dyson: in *Mechanical Behaviour of Materials IV*, J. Carlsson and N.G. Ohlson, ed., Pergamon, Oxford, 1984, pp. 289–95.
4. S.E. Ng, G.A. Webster, and B.F. Dyson: in *Advances in Fracture Research, ICF-5*, D. Francois, ed., Pergamon, Oxford, 1981, pp. 1275–83.
5. G. Eggeler, W. Tato, P. Jemmely, and B. de Mestral: *Scripta Metall. Mater.*, 1992, vol. 27, pp. 1091–96.
6. D.R. Hayhurst, F.A. Leckie, and J.T. Henderson: *Int. J. Mech. Sci.*, 1977, vol. 19, pp. 147–59.
7. D. Wu, E.M. Christian, and E.G. Ellison: *J. Strain Anal.*, 1984, vol. 19, pp. 209–20.
8. D.R. Hayhurst and J.T. Henderson: *Int. J. Mech. Sci.*, 1977, vol. 19, pp. 133–46.
9. B.J. Cane: in *Advances in Fracture Research, ICF-5*, D. Francois, ed., Pergamon, Oxford, 1981, pp. 1285–93.
10. D. McLean, B.F. Dyson, and D.M.R. Taplin: in *4th Int. Conf. on Fracture*, D.M.R. Taplin, ed., University of Waterloo Press, Waterloo, 1977, pp. 325–62.
11. D.R. Hayhurst and G.A. Webster: in *Techniques for Multiaxial Creep Testing*, D.J. Gooch and I.M. How, ed., Elsevier Applied Science, Amsterdam, 1986, pp. 137–75.
12. T.H. Hyde, A.A. Becker, W. Sun, and J.A. Williams: *Int. J. Press. Vessel. Pip.*, 2006, vol. 83, pp. 853–63.

13. T.H. Hyde, L. Xia, and A.A. Becker: *Int. J. Mech. Sci.*, 1996, vol. 38, pp. 385–403.
14. D.R. Hayhurst, P.R. Dimmer, and C.J. Morrison: *Philos. Trans. Royal Soc. Lond. A*, 1984, vol. 311, pp. 103–129.
15. A.M. Othman, D.R. Hayhurst, and B.F. Dyson: *Proc. Royal Soc. Lond. A*, 1993, vol. 441, pp. 343–58.
16. G.A. Webster, S.R. Holdsworth, M.S. Loveday, K. Nikbin, I.J. Perrin, H. Purper, R.P. Skelton, and M.W. Spindler: *Fatigue Fract. Eng. Mater. Struct.*, 2004, vol. 27, pp. 319–42.
17. B. Al-Abed, R. Timmins, G.A. Webster, and M.S. Loveday: *Mater. High Temp.*, 1999, vol. 16, pp. 143–58.
18. O. Kwon, C.W. Thomas, and D. Knowles: *Int. J. Press. Vessel. Pip.*, 2004, vol. 81, pp. 535–42.
19. W.D. Nix, J.C. Earthman, G. Eggeler, and B. Ilschner: *Acta Metall.*, 1989, vol. 37, pp. 1067–77.
20. T.H. Hyde, W. Sun, and A.A. Becker: *Int. J. Mech. Sci.*, 2000, vol. 42, pp. 401–423.
21. G.A. Webster, K.M. Nikbin, and F. Biglari: *Fatigue Frac. Eng. Mater. Struct.*, 2004, vol. 27, pp. 297–303.
22. B.J. Cane: in *Proceedings of the Int. Conf. on Mechanical behavior of Materials*, K.J. Miller and R.F. Smith, ed., Pergamon, Oxford, 1979, pp. 173–82.
23. R.L. Huddleston: *J. Press. Vessel Technol.*, 1985, vol. 107, pp. 412–29.
24. J. Lemaitre and J.-L. Chaboche: *Mechanics of Solid Materials*, Cambridge University Press, Cambridge, 1990.
25. Baldev Raj, S.L. Mannan, P.R. Vasudeva Rao, and M.D. Mathew: *Sadhana*, 2002, vol. 27, pp. 527–58.
26. S.C. Chetal, P. Chellapandi, P. Puthiyavinayagam, S. Raghupathy, V. Balasubramanian, P. Selvaraj, P. Mohankrishnan, and B. Raj: *Energy Procedia*, 2011, vol. 7, pp. 64–73.
27. W.D. Pilkey and D.F. Pilkey: *Peterson's Stress Concentration Factors*, 3rd ed., Wiley, Hoboken, NJ, 2008.
28. C.R. Calladine: *Proc. Royal Soc. Lond. A*, 1969, vol. 309, pp. 363–75.
29. L.M. Kachanov: in *The Theory of Creep*, A.J. Kennedy, ed., National Lending Library, Boston, 1967.
30. F. Abe, S. Nakazawa, H. Araki, and T. Noda: *Metall. Trans. A*, 1992, vol. 23A, pp. 469–77.
31. B.K. Choudhary, S. Saroja, K. Bhanu Sankara Rao, and S.L. Mannan: *Metall. Trans. A*, 1999, vol. 30A, pp. 2825–34.
32. E.I. Samuel, B.K. Choudhary, K. Bhanu Sankara Rao, and B. Raj: *Pressure Vessels and Piping: Materials and Properties*, Narosa, New Delhi, 2008, pp. 83–100.
33. F.A. Leckie and D.R. Hayhurst: *Acta Metall.*, 1977, vol. 25, pp. 1059–70.
34. M.F. Ashby and B.F. Dyson: in *Advances in Fracture Research*, R.S. Valluri, ed., Pergamon, Oxford, 1984, pp. 3–30.
35. B.F. Dyson and T.B. Gibbons: *Acta Metall.*, 1987, vol. 35, pp. 2355–69.
36. P. Lukas, P. Preclik, and J. Cadek: *Mater. Sci. Eng. A*, 2001, vol. 298, pp. 84–89.
37. S. Goyal, K. Laha, K.S. Chandravathi, P. Parameswaran, and M.D. Mathew: *Philos. Mag.*, 2011, vol. 91, pp. 3128–54.
38. I.J. Perrin and D.R. Hayhurst: *Int. J. Press. Vessel. Pip.*, 1999, vol. 76, pp. 599–617.
39. J.W. Hancock: *Met. Sci.*, 1976, vol. 10, pp. 319–25.
40. F.A. McClintock: *J. Appl. Mech.*, 1968, vol. 35, pp. 363–71.
41. D. Hull and D.E. Rimmer: *Philos. Mag.*, 1959, vol. 4, pp. 673–87.
42. M.F. Ashby, C. Gandhi, and D.M.R. Taplin: *Acta Metall.*, 1979, vol. 27, pp. 699–729.
43. J. Hancock: in *Topics in Fracture and Fatigue*, A. Argon, ed., Springer, New York, NY, 1992, pp. 99–144.
44. J.R. Rice and D.M. Tracey: *J. Mech. Phys. Solids*, 1969, vol. 17, pp. 201–217.
45. A.C.F. Cocks and M.F. Ashby: *Met. Sci.*, 1980, vol. 14, pp. 395–402.